THz quantum cascade lasers operating on the radiative modes of a 2D photonic crystal

Y. Halioua,[1,3] G. Xu,[1] S. Moumdji,[1] L. H. Li,[2] A. G. Davies,[2] E. H. Linfield,[2] and R. Colombelli[1,*]

[1]*Institut d'Electronique Fondamentale, Univ. Paris Sud, UMR 8622 CNRS, 91405 Orsay, France*

[2]*School of Electronic and Electrical Engineering, University of Leeds, Leeds LS2 9JT, United Kingdom*

[3]*e-mail: yacine.halioua@u-psud.fr*

**Corresponding author: raffaele.colombelli@u-psud.fr*

Received March 31, 2014; accepted May 11, 2014;
posted May 23, 2014 (Doc. ID 209162); published June 27, 2014

Photonic-crystal lasers operating on Γ-point band-edge states of a photonic structure naturally exploit the so-called "nonradiative" modes. As the surface output coupling efficiency of these modes is low, they have relatively high Q factors, which favor lasing. We propose a new 2D photonic-crystal design that is capable of reversing this mode competition and achieving lasing on the radiative modes instead. Previously, this has only been shown in 1D structures, where the central idea is to introduce anisotropy into the system, both at unit-cell and resonator scales. By applying this concept to 2D photonic-crystal patterned terahertz frequency quantum cascade lasers, surface-emitting devices with diffraction-limited beams are demonstrated, with 17 mW peak output power. © 2014 Optical Society of America

OCIS codes: (140.5965) Semiconductor lasers, quantum cascade; (140.7260) Vertical cavity surface emitting lasers; (230.5298) Photonic crystals; (140.3070) Infrared and far-infrared lasers.

http://dx.doi.org/10.1364/OL.39.003962

Photonic-crystals (PhCs) are artificial dielectric structures that can confine or bend light according to a predetermined design [1]. The application of this concept to semiconductor devices has led to a plethora of applications. Lasers, in particular, can benefit from PhCs owing to a PhC's ability to confine light strongly [2] and to both control internal light propagation [3] and the emission properties [4].

In the terahertz (THz) frequency range of the electromagnetic spectrum, several PhC design strategies have been applied to quantum cascade laser (QCL) technologies in recent years [5,6]. The goal has been to improve the shape and quality of the strongly divergent emission [5,6] and the power efficiency of the devices by using the confinement and/or the dispersion properties of periodically patterned (in 1D or 2D) metal-semiconductor-metal structures. To date, a coherent single-lobed emission with reduced divergence has been obtained in edge-emitting devices, using third-order distributed feedback (DFB) gratings [7,8], and in surface-emitting devices, using 2D PhCs [9,10] and second-order DFBs [11,12]. However, efficient power extraction and, hence, wall-plug efficiency (WPE) from DFB- or PhC-patterned QCLs has been elusive. WPEs for these devices fall well below the current state-of-the-art for THz QCLs exploiting unpatterned single-plasmon waveguides, where values in the 0.5%–1% range are currently achieved at 10 K [5].

The problem in achieving high WPE has a fundamental origin. 1D and 2D PhCs support two classes of modes at the high symmetry points in the band structure where PhC lasers usually operate. These modes are associated with either symmetric or antisymmetric electric field profiles on the scale of the unit cell. When located above the light line, both modes will give rise to emission but will result in constructive or destructive interference. THz frequency QCLs (and indeed all QCLs) are TM polarized, i.e., the electric field is aligned parallel to the growth (z) axis. Since surface emission originates from the in-plane components of the field in the holes/slits of 2D/1D PhCs, it is only the magnetic field component that sources the radiation [13]. As a general rule, antisymmetric modes with respect to E_z are symmetric with respect to the in-plane **H** field in the slits/holes of the DFB/PhC and are, hence, labeled "radiative." Conversely, symmetric E_z modes are antisymmetric with respect to the in-plane **H** field and are, hence, termed "nonradiative." In fact, radiative modes at the Γ point ($k_{\text{in-plane}} = 0$) naturally exhibit an emission maximum in the direction normal to the device surface. As a consequence, the following relation is always true: $Q_{\text{vertical non-radiative}} > Q_{\text{vertical radiative}}$. Since the in-plane Q factor, $Q_{\text{in-plane}}$, is of the same order of magnitude for all the modes, the laser competition, which favors modes with the highest total Q factor, supports the nonradiative modes, leading to low output power.

In [14], a methodology was demonstrated that reverses the mode competition in favor of the radiative modes for 1D periodic photonic structures. It exploits 1D ridge gratings with graded periodicity (graded photonic heterostructures, GPH), leading to increase in both the power slope efficiencies and WPEs and single-lobed surface emission [15]. This concept relies crucially on the existence of a full photonic gap [Fig. 1(a)]: when the grating period a is slightly decreased from the center to the edge of the device, the bandgap blueshifts, and the resulting effective potential for photons [16] resembles a type-II electronic quantum well [Fig. 1(b)]. The radiative modes—which in 1D correspond to the upper branch—are therefore spatially confined and exhibit elevated $Q_{\text{in-plane}}$. In contrast, the nonradiative modes are delocalized to the device edges, where judiciously designed absorbing boundaries greatly lower the $Q_{\text{in-plane}}$. The net result is that the total Q factor (Q_{total}) of the radiative mode is now the largest, and lasing occurs on a high-power radiative mode.

However, a drawback of this concept arises from the narrow laser ridge (80–120 μm) typically used in QCL devices, which leads to elliptical far fields (diffraction

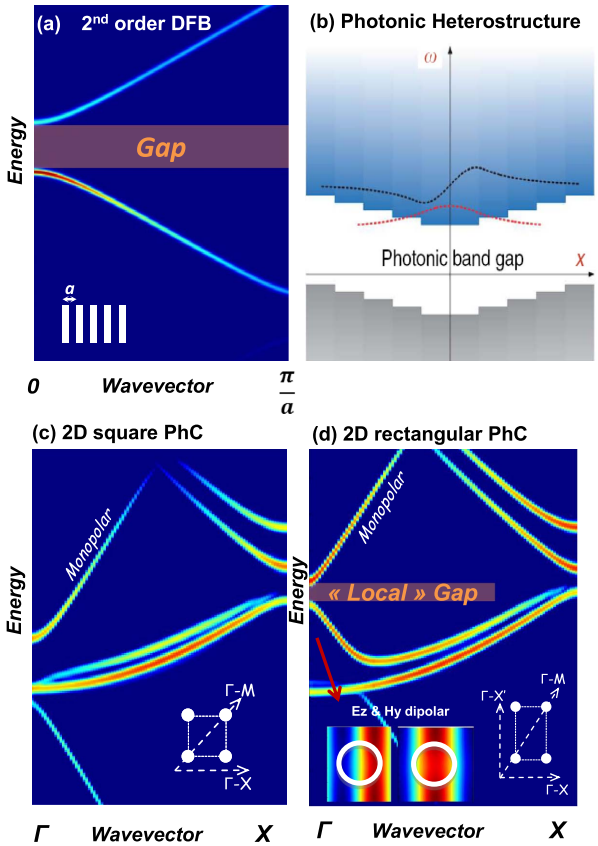

Fig. 1. (a) Typical bandstructure of a 2nd order metal/semiconductor DFB grating of period a. The upper band (at $k = 0$) is identified with the radiative mode, the lower band with the non-radiative mode. (b) Schematic representation of the grading effect in a GPH ($a_{i+1} = a_1 \cdot \alpha$, $\mathrm{abs}(\alpha) < 1$) from center to the edges. A "photonic well" ensures confinement of the radiative modes (red and black dashed lines) while the non-radiative modes are displaced, from the band center to the edges. (c) Dispersion curve of a 2D square metal/semiconductor PhC. Inset: Brillouin zone of a square lattice (d) Band structure of a PhC with anisotropic lattice (lattice $= 28 \times 36\ \mu\mathrm{m}^2$, hole radius $= 8\ \mu\mathrm{m}$). The two upper branches are identified (from top to bottom) with the non-radiative (monopolar) and radiative modes (dipolar), respectively, according to their lattice field profiles. Their dispersion, in a portion of the Brillouin zone around the Γ-point, is similar to a 2nd order DFB. Bottom left inset: E_z and H_y components of the dipolar mode. The unit-cell anisotropy (bottom right inset) splits the degeneracy along orthogonal directions of the lattice, hence the $\Gamma - X'$ direction is introduced. However, this region of the reciprocal space is not relevant in this context since the modes of interest oscillate along $\Gamma - X$.

limited) and also prevents the scaling up of output power. The extension of the GPH concept to 2D systems would solve both problems simultaneously, since the device surface area would increase. However, at a first sight, a direct transposition of the GPH concept appears impossible since a 2D connected PhC lacks a photonic bandgap for TM polarization. In this Letter, we show that this can be circumvented: it is possible to map the desired 2D GPH onto two uncoupled 1D GPHs and successfully develop 2D PhC lasers operating on radiative modes. We call this device architecture a "2D GPH resonator."

Our starting point is a square PhC lattice of air holes in the top metal plate of a metal-metal waveguide (the waveguide geometry used for high-performance THz QCLs [17]). The important modes—both located at the Γ point of the photonic band structure [Fig. 1(c)]—are the two degenerate dipolar and the single monopolar modes. They are radiative and nonradiative, respectively; the latter being the naturally lasing mode [8,9].

In order to mimic the 1D GPH case, a photonic bandgap is needed. The solution is to introduce anisotropy on the lattice scale. By using a rectangular rather than a square photonic lattice [Figs. 1(c) and 1(d)], it is possible to tailor the frequencies and curvatures of the dispersion curves of the dipolar and monopolar modes. Figure 1(d) shows that with a correctly designed rectangular lattice, it is possible to reproduce the typical second-order DFB dispersion curve in a portion of the Brillouin zone around the Γ point. Comparison with Fig. 1(c) (the square lattice case) highlights the emergence of a local bandgap when a rectangular photonic lattice is used.

A spatial Fourier transformation of the field profile of any PhC mode reveals in general the distribution of k vectors in reciprocal space. In our case, it shows that the monopolar mode results from oscillations/coupling of Bloch harmonics lying on the two axes of the lattice, while each of the degenerate dipolar modes rely on oscillations on only one axis [18]. The first consequence of this is that both dipolar modes can be considered, to a certain extent, as equivalent to 1D modes [this can also be seen in the field profiles shown as inset of Fig. 1(d)]. It appears therefore legitimate to adjust the period along one axis of the PhC in order to ensure lateral confinement of the "pseudo-1D" dipolar mode, mimicking the strategy used for 1D GPH resonators. This is achieved by grading the lattice spacing with the recursive rule, $a_{i+1} = a_i \cdot \alpha$, where a_i is the period at the position i of the photonic lattice. Note: contrary to a 1D GPH, $|\alpha| > 1$, since the radiative mode is the lower energy one and has a negative dispersion band slope.

The second consequence revealed by the Fourier analysis is that any change affecting the coupling constants along one PhC axis will always have an impact on the monopolar mode, but it will not affect the dipolar mode residing along the other axis. This peculiarity permits to further strengthen the mode competition in favor of the dipolar radiative mode, which is quantified by the ratio $Q_{\text{total-dipolar}}/Q_{\text{total-monopolar}}$ (the quadrupolar mode is not considered since it is located outside the QCL gain bandwidth) by introducing anisotropy at the resonator level too. Implementing PhC resonators with an overall rectangular shape [see Fig. 2(a) for a photograph of a typical device] has the following consequence: along the transverse short side (the y axis), the Bloch harmonic oscillations become too weak to sustain the monopolar mode efficiently, and its $Q_{\text{in-plane}}$ is drastically reduced (from 110 to 40 in this case). Importantly, this does not affect the dipolar mode, which oscillates on the longitudinal x axis (chosen arbitrarily as the grading axis), and it is effectively decoupled.

To demonstrate the 2D GPH concept, we used a GaAs/AlGaAs QCL structure based on a modified resonant phonon active region design [7] with a peak gain at ~2.9 THz (wafer L916). The PhC [Fig. 2(a)] comprises a 20×14

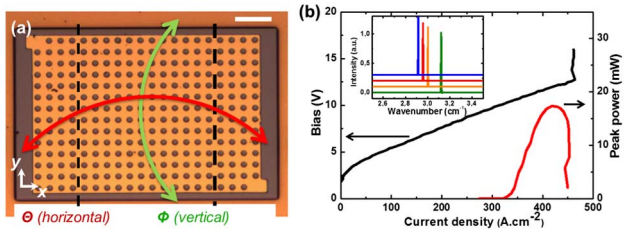

Fig. 2. (a) Image of the sample. The gray surrounding zone is an absorbing region. The scale bar (top right) is 100 μm long. Green and red arrows define the scanning angles used in beam profiling measurements. (b) Typical current density-voltage and current density-output power curves. The output peak power is typically ∼15–17 mW. The inset shows the frequency of the laser emission for various scaling parameters S of the PhC: 0.95, 1, 1.016 and 1.032, respectively. The PhC lasers typically exhibit single mode operation.

hole resonator, with lattice parameters $a_x = 28.3$ μm and $a_y = 30.75$ μm (rectangular lattice basis). The α (grading) parameter in the x direction is 1.045, but only the period of the outermost four holes—on each side—is graded, as delineated by the black dashed lines. Absorbing boundary conditions—following the proven methodology of [9]—are implemented at the device boundaries to avoid whispering-gallery-like modes.

Typical light-current-voltage (LIV) characteristics, acquired at 1% duty cycle, are shown in Fig. 2(b). The inset of Fig. 2(b) shows the laser emission spectra for PhCs with various lattice parameters, obtained by applying a scaling parameter S to the design. The emission is typically spectrally monomode and, as expected from the theory, the frequency linearly blueshifts with the inverse of the scaling parameter. The threshold current densities at cryogenic temperature are ∼320 A. cm^{-2} (approximately 0.8 A in absolute current), and the peak output powers range from ∼12 to 17 mW (at 8 K). The slope efficiency is ∼74 mW/A, and the highest recorded WPE is ∼0.13%. These output powers and WPEs are one order of magnitude higher than typically obtained from standard PhC THz lasers operating on nonradiative modes [10]. An estimate of the outcoupling efficiency defined as $Q_{\text{vertical}}/Q_{\text{total}}$ corroborates this observation, with Q_{vertical} of the nonradiative modes being typically a few thousand, while radiative modes exhibit Q_{vertical} of ∼50–100. The maximum operating temperature has been measured as being equal to 105 K.

A typical experimental far-field profile is shown in Fig. 3(a). It exhibits a clear single-lobed emission of ∼7° × 10° divergence (defined as the angular FWHM), which compares well with the recent state-of-art [5]. This value is only marginally larger than predicted by the diffraction limit, 6.5° × 9°, according to the formula, $\Delta\theta = 2 \cdot \text{atan}(\lambda/\pi L)$, based on a device size of 565 μm × 400 μm. The single-lobed emission is the definitive proof that the device is operating on radiative modes, while the near-diffraction limited far-field divergence suggests that almost every hole in the structure participates in the emission. This demonstrates that it is sufficient to grade only a few periods (four in our case) at the edges of the structure to induce the spatial confinement of a radiative dipolar mode.

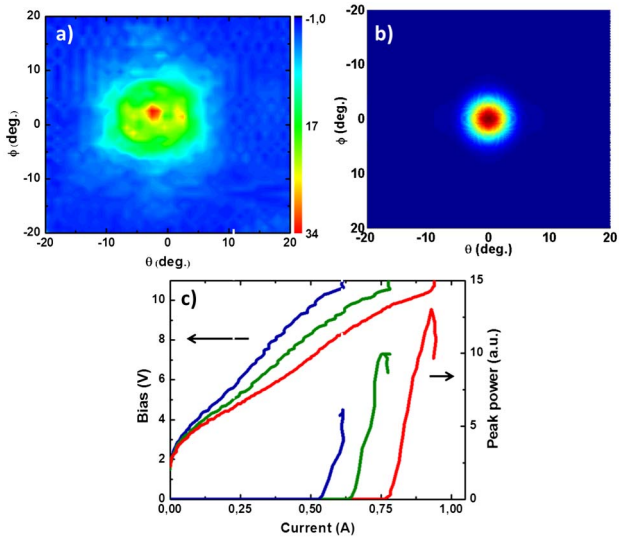

Fig. 3. (a) The measured far-field pattern for a typical PhC laser operating on the radiative mode. The far-field emission is naturally single-lobed, and the divergence angles (∼7° × 10°) are close to the diffraction limit expected from the size of the device. (b) Numerical simulation—obtained by FDTD analysis—of the emission far-field of the analyzed device. (c) Current-voltage and current-output power curves for various sizes of PhCs. As the lateral size of the resonator is increased from 414 μm (blue curve) to 533 μm (green curve) and 651 μm (red curve), the peak power increases from 6 mW to 9.5 mW and 13 mW, respectively, at 8 K.

Polarized far-field measurements (data not shown) demonstrate the high degree of polarization of the laser emission. This is a direct consequence of the device operation on a dipolar (radiative) mode that—as suggested above—can be considered equivalent to a 1D mode. In fact, the dipolar mode exhibits a single in-plane magnetic field component perpendicular to the long axis of the device. The prediction of numerical finite-difference time-domain simulations is in excellent agreement with the measurements [Fig. 3(b)] and remove any remaining ambiguity about the nature of the lasing mode.

In a complementary study, we explored the tolerance of the design when the resonator is made more square, i.e., for an increasing number of holes in the transverse resonator direction (y). With the same laser active region design (but a different wafer, L946), we have implemented 20×14, 20×18, and 20×21 hole 2D GPH devices. The typical LIV characteristics are shown in Fig. 3(b). Although the peak output power (at 8 K) increases with device size as expected (6, 9, and 13 mW, respectively), it is interesting to note that this increase is superlinear: the surface area scales as 1/1.3/1.6, while the peak power scales as 1/1.5/2.1. This is probably related to the absorbing boundary conditions whose effect becomes more dominant for smaller devices. In fact, the maximum WPE is 0.14% for the largest device, while it is only 0.09% for the smallest one. As for the previous devices, the emission is nearly single mode, and the emission far-field patterns are single lobed (data not shown). Even the almost square resonator devices operate on the radiative mode, suggesting that the grading procedure only (plus the anisotropy at the unit cell scale) is sufficient to correctly engineer a 2D GPH.

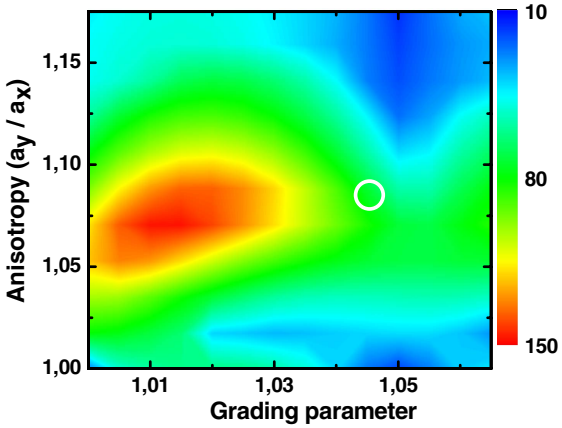

Fig. 4. In plane Q factor as a function of the lattice anisotropy, defined as the ratio of a_y/a_x (a_x being the grading axis) and grading parameter α, the rule $a_{i+1} = a_i \cdot \alpha$ being applied to the outermost four lateral holes. The color map shows an optimum operation point in a region corresponding to 1.075 anisotropy and grading $\alpha = 1.015$. The white circle locates the operating point of the reference PhC used in the article.

We now compare the experimental measurements with the predictions obtained from numerical simulations. Figure 4 shows a color map of the in-plane Q factor ($Q_{\text{in-plane}}$) of the dipolar mode as a function of the lattice anisotropy (defined as a_y/a_x) and of the grading parameter α (defined with the recursive rule $a_{i+1} = a_i \cdot \alpha$, as explained above), assuming that only the four outermost holes are graded. This shows that a large increase of $Q_{\text{in-plane}}$ can be achieved for the dipolar mode from ~40 (square, ungraded PhC) to ~145 for an optimal configuration where $\alpha \approx 1.015$ and the lattice anisotropy equals ≈1.075. It appears that the optimum grading parameter was slightly overestimated when fabricating the devices discussed in Figs. 2 and 3 (marked by the white circle in Fig. 4). However, even in this configuration, the devices still operate on the radiative mode. This is because (1) the resonator was designed to be anisotropic, and (2) the grading not only confines the radiative mode, but also delocalizes the nonradiative mode toward the lossy resonator edges.

In conclusion, we have demonstrated a new type of PhC design exploiting lattice and resonator anisotropy. This design was used to address mode competition between nonradiative and radiative modes in 2D THz periodic devices. As a result, our devices provide output beams with extremely low divergence ($7° \times 10°$). However, although we demonstrate reasonable output peak powers (17 mW) and WPEs (0.13%), these remain lower than might be expected, and particular attention will be given in the next generation of devices to Q_{vertical}, focusing on the coupling efficiency $\eta = Q_{\text{vertical}}/(Q_{\text{vertical}} + Q_{\text{in-plane}})$. We have also demonstrated that there is design tolerance to changes in the patterned structures and that one can at least double the output power by increasing the resonator's lateral size. In fact, the methodology proposed here to manage mode competition using lattice and resonator anisotropy is of general relevance, in particular in contexts where the symmetry of the PhC modes plays a crucial role.

We thank Nathalie Isac for technical help with the wafer bonding process. We acknowledge support from the ANR projects PHASE-LOCK and DELTA. We also acknowledge support of the EPSRC, and the EC programs *NOTES* and *TOSCA*. AGD acknowledges support of the Royal Society and Wolfson Foundation. This work was partly supported by the French RENATECH network.

References and Notes

1. J. D. Joannopoulos, S. G. Johnson, J. N. Winn, and R. D. Meade, *Photonic Crystals: Molding the Flow of Light*, 2nd ed. (Princeton University, 2008).
2. Y. Akahane, T. Asano, B. Song, and S. Noda, Nature **425**, 944 (2003).
3. M. Notomi, K. Yamada, A. Shinya, J. Takahashi, C. Takahashi, and I. Yokohama, Phys. Rev. Lett. **87**, 253902 (2001).
4. M. Narimatsu, S. Kita, H. Abe, and T. Baba, Appl. Phys. Lett. **100**, 121117 (2012).
5. C. Sirtori, S. Barbieri, and R. Colombelli, Nat. Photonics **7**, 691 (2013).
6. X. Checoury, R. Colombelli, and J. M. Lourtioz, in *Compact Semiconductor Lasers*, ed. (Wiley, 2014), pp. 91–149.
7. M. I. Amanti, M. Fischer, G. Scalari, M. Beck, and J. Faist, Nat. Photonics **3**, 586 (2009).
8. T. Y. Kao, Q. Hu, and J. L. Reno, Opt. Lett. **37**, 2070 (2012).
9. Y. Chassagneux, R. Colombelli, W. Maineult, S. Barbieri, H. E. Beere, D. A. Ritchie, S. P. Khanna, E. H. Linfield, and A. G. Davies, Nature **457**, 174 (2009).
10. G. Sevin, D. Fowler, G. Xu, F. H. Julien, R. Colombelli, H. E. Beere, and D. A. Ritchie, Electron. Lett. **46**, 1513 (2010).
11. J. A. Fan, M. A. Belkin, and F. Capasso, Opt. Express **14**, 11672 (2006).
12. S. Kumar, B. S. Williams, Q. Qin, A. M. Lee, Q. Hu, and J. L. Reno, Opt. Express **15**, 113 (2007).
13. G. Xu, R. Colombelli, S. P. Khanna, A. Belarouci, X. Letartre, L. Li, E. H. Linfield, A. G. Davies, H. E. Beere, and D. A. Ritchie, Nat. Commun. **3**, 952 (2012).
14. G. Xu, Y. Halioua, S. Moumdji, R. Colombelli, H. Beere, and D. Ritchie, Appl. Phys. Lett. **102**, 231105 (2013).
15. E. Istrate and E. H. Sargent, Rev. Mod. Phys. **78**, 455 (2006).
16. All modeling studies were carried out with 2D FDTD modeling using Lumerical Software (www.lumerical.com).
17. J. Vučković, M. Lončar, H. Mabuchi, and A. Scherer, IEEE J. Quantum Electron. **38**, 850 (2002).
18. Y. Chassagneux, R. Colombelli, W. Maineult, S. Barbieri, S. P. Khanna, E. H. Linfield, and A. G. Davies, Appl. Phys. Lett. **96**, 031104 (2010).